Journal of Archaeological Science 63 (2015) 94–103

Contents lists available at ScienceDirect

Journal of Archaeological Science

journal homepage: http://www.elsevier.com/locate/jas

Multi-emission luminescence dating of heated chert from the Middle Stone Age sequence at Sodmein Cave (Red Sea Mountains, Egypt)

Christoph Schmidt [a, b, *], Karin Kindermann [c], Philip van Peer [d], Olaf Bubenzer [b]

[a] Chair of Geomorphology, University of Bayreuth, 95440 Bayreuth, Germany
[b] Institute of Geography, University of Cologne, Albertus-Magnus-Platz, 50923 Köln, Germany
[c] Institute of Prehistoric Archaeology, CRC 806, African Archaeology, University of Cologne, Bernhard-Feilchenfeld-Straße 11, 50969 Köln, Germany
[d] Prehistoric Archaeology Unit, KU Leuven, Celestijnenlaan 200e, Box 2409, 3001 Leuven, Belgium

ARTICLE INFO

Article history:
Received 21 April 2015
Received in revised form
17 August 2015
Accepted 18 August 2015
Available online 20 August 2015

Keywords:
Luminescence dating
Burnt chert
Burnt flint
Egypt
Out of Africa II
Middle Stone Age

ABSTRACT

Sodmein Cave in Egypt is one of the rare archaeological sites in north-eastern Africa conserving human occupation remains of a period most relevant for the 'Out of Africa II' hypothesis. This underlines the need for establishing a chronological framework for the more than 4 m of stratified sediments ranging from the Middle Stone Age (MSA) to the Neolithic. The lowest layer J hosts huge fireplaces, from which we report luminescence ages of heated chert fragments unearthed from different depths. The 'multi-emission' dating approach – using both the blue and red TL of each specimen as well as the OSL emission of one sample – allowed identifying the most reliable ages. Samples yield ages between <121 ± 15 ka (maximum age) and 87 ± 9 ka. These data evidence human presence at the site during MIS 5. For integrating Sodmein Cave into the actual discussion of the dispersal patterns of modern humans and to identify potential connections with other sites in the Nile Valley and in the Middle East, a sound and reliable chronology is indispensable.

1. Introduction

Understanding the movement of modern humans through and out of Africa from the centre of the origin is a major research issue. It is conventionally assumed that the habitat expansion accompanied by the interglacial period MIS 5e relaxed ecological constrains to such a degree that the movement of modern humans through north-eastern Africa towards the Levant became feasible (e.g., Derricourt, 2006; Beyin, 2011; Grove, 2015; Pagani et al., 2015). Stratigraphic and secure dating evidence, however, from Late Pleistocene archaeological sites of north-eastern Africa is very limited, and well-dated Palaeolithic sites still remain desirable. One of these rare sites in this time range is Sodmein Cave in Egypt (Fig. 1). This outstanding cave stratigraphy is – beside the Haua Fteah Cave in Libya – the only living site in this time range in north-eastern Africa. In contrast, the contemporaneous sites from the Nile Valley are mostly raw material procurement sites (cf. Vermeersch, 2002).

Sodmein is located about 40 km north–west of the city of Quseir in an isolated Tertiary limestone complex (Djebel Umm Hammad/Djebel Duwi) of the Red Sea Mountains (Vermeersch et al., 1994; Kindermann et al., 2013). This elongated Eocene limestone ridge runs almost parallel to the Red Sea trough and is surrounded as well as underlain by the basement rocks of the Red Sea Mountains. Sodmein Cave is situated on the northern flank of the breakthrough of Wadi Sodmein through Djebel Duwi, around 17 m above the present wadi floor (Fig. 2).

The cave was visited regularly by humans during the Late Pleistocene and later on during the Holocene. The excavated sequence comprises more than 4 m stratified human occupation remains, spanning from the Middle Stone Age (MSA) through the Neolithic (Moeyersons et al., 2002). As a consequence of its position in a shelter and the recent extreme arid climatic conditions, the archaeological sequence is on the one hand devoid of any fluvial disturbances, but features on the other hand well preserved organic material (e.g., faunal material). Heated chert fragments associated with an ancient hearth in layer J provided the opportunity to determine the time of the last firing by luminescence methods and thus to add to the chronological placement of this site. Several luminescence emissions (blue thermoluminescence, BTL, red thermoluminescence, RTL, and optically stimulated luminescence, OSL) were recorded for each sample and used for age calculation to

* Corresponding author. Chair of Geomorphology, University of Bayreuth, 95440 Bayreuth, Germany.
E-mail address: christoph.schmidt@uni-bayreuth.de (C. Schmidt).

http://dx.doi.org/10.1016/j.jas.2015.08.016
0305-4403/

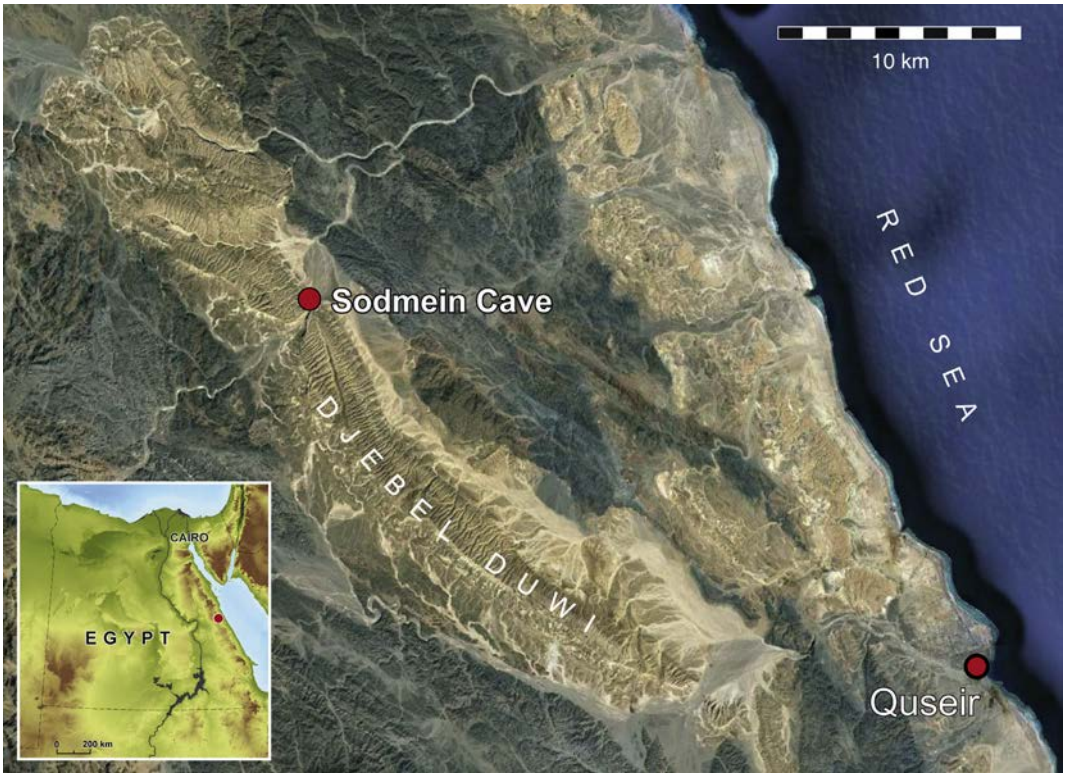

Fig. 1. Location of Sodmein Cave and Djebel Duwi in the Egyptian Eastern Desert. The detail map illustrates the research area in Egypt (satellite image Google earth 2014; the topography of the detail map is based on SRTM-DEM, brown = high and green = low).

increase the level of confidence of the chronological information. The obtained ages represent new constraints for human presence in the context of the much-discussed 'Out of Africa II' debate and may further help in tracing possible interactions of human activity and environmental changes (Derricourt, 2006; Beyin, 2011; Wurz and Van Peer, 2012).

2. Previous research and chronometric dating

Sodmein Cave was discovered in 1979 by M. Prickett during a survey (Prickett et al., 1979), but systematic research did not begin until the 1990s by the Belgian Middle Egypt Prehistoric Project (BMEPP) of the University of Leuven (Moeyersons et al., 2002). Since 2010, fieldwork has resumed in this area of the Eastern Desert through cooperation between the Universities of Cologne and Leuven under the aegis of the Collaborative Research Center "Our Way to Europe" (CRC 806).

Multiple human occupation events are represented throughout the Late Pleistocene stratigraphic sequence of the cave. Generally, the archaeological remains are situated near the entrance of the cave at the interface of angular rockfall deposits and more organic backfill sediments that accumulated inside the cave. The entire depositional sequence rests on coarse limestone boulders which represent the initial roof collapse creating the present cave. MSA levels are found from layer J at the base through layer G (see Fig. 3). Layers J and I contain Early Nubian Complex[1] occupation debris, whereas Late Nubian Complex and transitional levels occur in G. Layer H is archaeologically sterile.

Mercier et al. (1999) dated six heated chert fragments from two large blocks located at the western and eastern end of a large hearth in layer J. The samples come from what was called at the time the upper and middle ash layer, respectively (see Fig. 3). Technically, a multiple-aliquot additive-dose approach together with a second-glow regenerative-dose growth curve (for supra-linearity correction) was applied to crushed coarse grain material from the inner cores of the chert fragments (cf. Valladas, 1992; Mercier et al., 1995). All six calculated TL ages are identical within confidence intervals, giving an overall mean of 118 ± 8 ka and placing this human occupation in Sodmein Cave early in isotopic stage 5. Within measurement uncertainty, these ages unfortunately do not allow us to distinguish between individual burning phases. Radiocarbon dating of charcoal from organic layer G gave minimum ages of ≥45,000 BP and ≥30,000/≥44,500 BP. At the interface of overlying layers E and D occurs Upper Palaeolithic artefact material which was dated by ^{14}C to 25,200 ± 500 BP. The subsequent layers B and C were described by the BMEPP as Neolithic layers and radio-carbon dating gave ages between 6320 ± 100 and 7470 ± 110 BP (Mercier et al., 1999; Moeyersons et al., 2002).

3. Critical review of the stratigraphic position of the luminescence samples

The fire pit with which the dated samples are associated has been redug several times. In Fig. 3, the south profile along the 38 m gridline of trench B as published in the paper by Mercier et al. (1999) is redrawn and completed with the stratigraphic positions of the new samples that are reported here. At the time, three burning phases were distinguished of which the most recent has been dug into layer J from a surface that existed during the

[1] The Nubian Complex is a techno-complex of north-eastern Africa which is characterised technologically by the Nubian Levallois methods for points and the classical Levallois method for flake production (Van Peer, 1998; Van Peer and Vermeersch, 2000).

Fig. 2. Wadi Sodmein with the cave during the excavation in 2010; the present wadi floor is located around 17 m below the cave entrance.

initial buildup of layer I. The central portion of this fire pit, as it was redrawn in much more detail during the 2010 field campaign when the new luminescence samples were taken, is shown in Fig. 3c. Since the original recording in 1995, the profile has collapsed in certain areas, but, essentially, the 1995 observations are confirmed. In a clearer fashion, however, the 2010 profile shows the stratigraphic distinction between the lower and the middle hearth. The former appears to occur in a small pit-like feature. During the 1999 excavation campaign its more or less horizontal extension to the north–east of the section drawn here was observed at an elevation of about 14.2 m. It is cut by the middle hearth which, on the 2010 profile, seems to comprise two burning phases separated by a layer of consolidated grey ashes overlain by coarse limestone clasts.

Sample ME93/489 was located at the eastern extremity of the fire pit where its ash infilling accumulates against and partially overlies one of the large limestone boulders at the base of the cave sequence which delimits a basin of deposition for the hearth deposits (Fig. 3b). This burned chert fragment was found on top of the limestone boulder during the first excavation in 1993. Mercier and colleagues attributed this sample to the upper hearth phase, based on the lay-out of the fire pit as drawn in Fig. 3b. However, it is important to remark that the limestone boulder has been projected into this profile recording. At the time when the profile was drawn, the south profile in this area of trench B had been cut back to the 36 m gridline. Thus, neither the precise lay-out nor the precise correlation of the ash deposit on top of the limestone boulder with the core of the fire pit to the west is known. Based on the new stratigraphic recording during the 2010 campaign, an association with the middle hearth seems more feasible (see Fig. 4).

Sample ME95/56 was retrieved from an elevation of 15.3 m at an almost identical position as the present sample SodTL1,[2] both samples being associated with the older phase of the middle hearth. If the re-allocation of ME93/498 is correct, these three samples each provide an age estimation of the first burning phase of the middle hearth.

Samples SodTL2–SodTL4 occur in association with a layer of limestone clasts at the base of ash deposits of the second burning phase of the middle hearth. They might be associated with this event, but, on the other hand, they may also have been reworked from the older burning phase. Only SodTL2 provided an age estimate (see below).

4. Luminescence dating of heated chert

Luminescence dating can provide chronometric information of crucial importance for the temporal assessment of a site's occupation beyond the dating range of the radiocarbon method and in environments lacking suitable organic materials. In particular, luminescence dating of heated lithic artefacts enables direct determination of human activity in the context of hearth usage, provided that natural causes of fire can be precluded (Richter et al., 2009; Schmidt, 2013).

From the five samples (SodTL0–SodTL4) unearthed from the hearth in layer J (Fig. 3) and selected for their greyish–pinkish appearance induced by heating, only three proved suitable for luminescence dating. The others either contained no chert or the material was too calcined and brittle from heating (>540 °C;

[2] A setback of the 38 N profile due to collapses in the 15 years between the two sampling seasons must be taken into account.

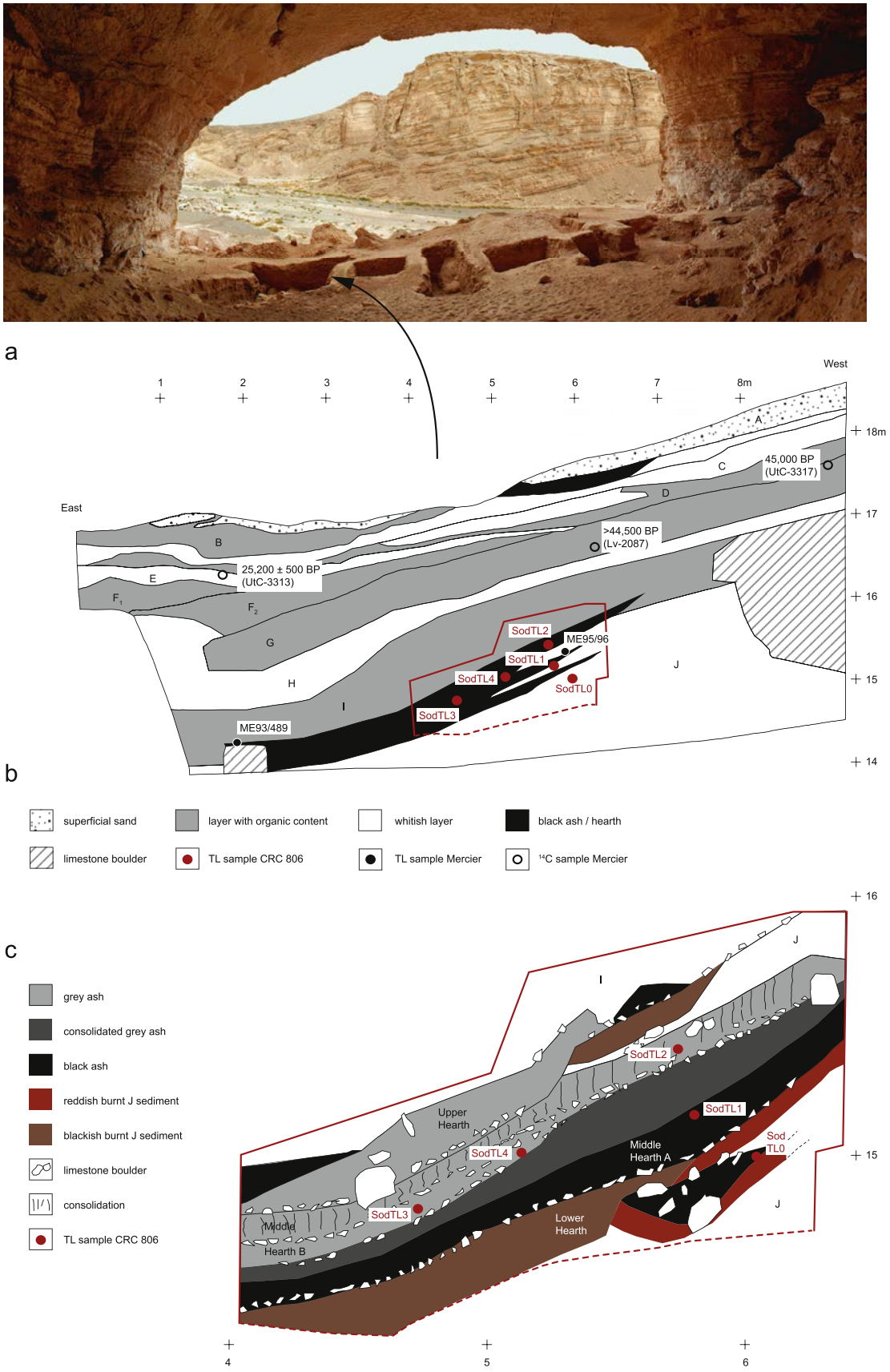

Fig. 3. (a) View eastward from the back of Sodmein Cave over the archaeological trenches. (b) Stratigraphy of the south profile along the 38 m gridline of trench B, redrawn after Mercier et al. (1999). The location of the new luminescence samples SodTL0–SodTL4 is added. The red polygon indicates the area of the section that was redrawn in 2010 and the lower red dashed line below the red polygon indicates the base of the new recorded hearth profile. (c) Detailed section drawn in 2010 with exact positions of the new luminescence samples SodTL0–SodTL4.

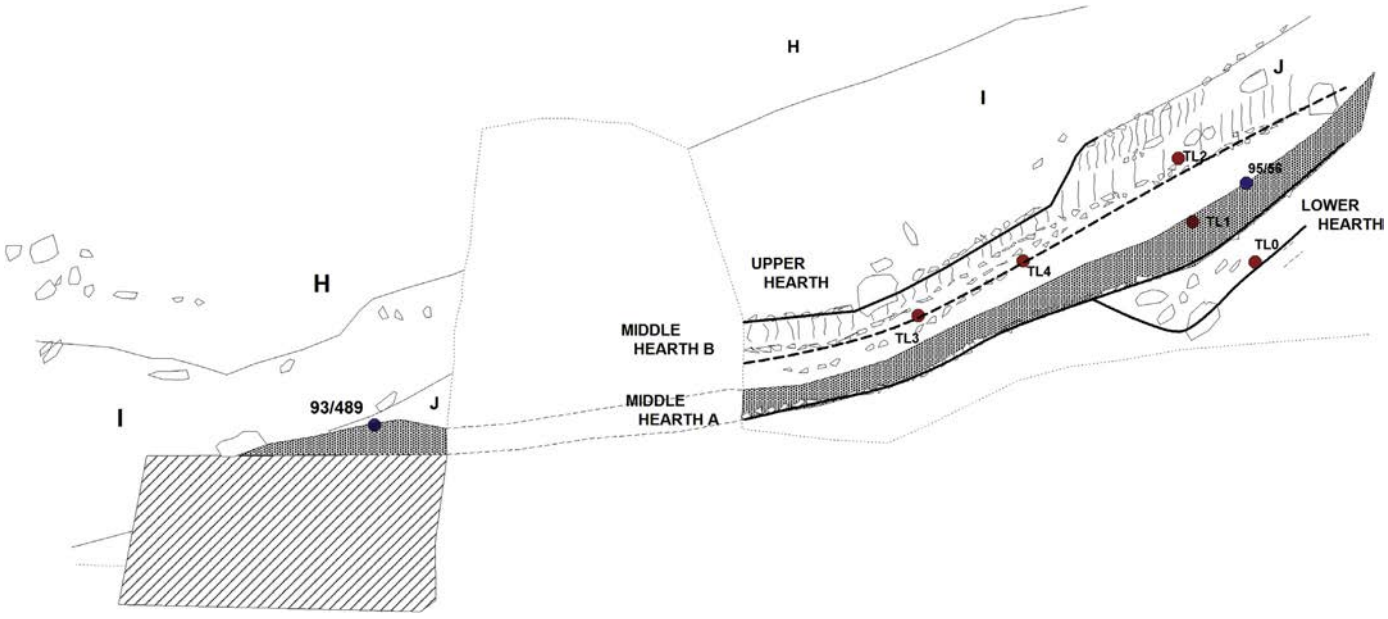

Fig. 4. Stratigraphic sketch of the fire pit indicating the different burning phases or 'hearths' and the associations of the 1995 BMEPP TL samples and the recent luminescence samples with the former. Note that sample 93/489 is now associated with the middle hearth, and not the upper hearth as published by Mercier et al. (1999).

Richter and Temming, 2006), so that they were excluded.

4.1. Sample preparation

Sample preparation included mechanical discarding of a ≥2 mm rim with a water-cooled diamond saw to remove material influenced by light and external β-radiation. The inner cores of the chert fragments were gently crushed to grain sizes of 100–200 μm in a steel mortar and subsequently treated with 10% HCl to remove carbonates. Determination of α-efficiency was carried out on fine-grained material (~4–11 μm), which was obtained by settling in acetone using Stokes' Law.

4.2. Instrumentation and measurement conditions

All luminescence measurements were conducted with automated Risø TL/OSL DA-20 readers equipped with $^{90}Sr/^{90}Y$ β-sources delivering dose rates between ~0.09 and ~0.15 Gy s^{-1}. Optical stimulation of chert samples was performed using blue diodes (470 ± 30 nm) at 130 °C for 80 s. Luminescence signals were detected with an EMI 9235QB photomultiplier-tube. Depending on the detected emission, one of the following optical filters was inserted between sample and photomultiplier: (1) a 7.5 mm Hoya U340 glass filter (OSL; transmission range 275–375 nm), (2) a Semrock Brightline HC 475/50 interference filter (BTL; transmission range 450–500 nm) or (3) a Chroma D630-60 interference filter (RTL; transmission range 600–660 nm). The quantum efficiency of the photomultiplier used here is highest in the UV/blue spectral range (200–350 nm; 25–30%) and reduced (~1% at 600 nm) in the orange–red range as relevant for RTL. RTL signal intensities were nevertheless well above the level of blackbody radiation and instrumental background. Heating rates were set to 5 K s^{-1} for BTL and 2 K s^{-1} for RTL measurements, and TL readout was conducted in N_2 atmosphere. The background due to blackbody radiation was immediately measured during a second TL readout and subtracted. The central 8 mm of stainless steel discs were covered with sample material; fine-grained material was deposited as a monolayer onto aluminium discs.

For α-efficiency determination, the luminescence intensities induced by single α- and β-doses (sensitivity-corrected by a β-dose) in the linear part of the dose response were compared to calculate the *b*-value (Bowman and Huntley, 1984); the fine grain material was heated to 500 °C prior to that. Alpha-irradiation was conducted in vacuum (~10 mbar) with a ^{241}Am source (~30 MBq, dose rate 0.167 ± 0.005 Gy s^{-1}; 0.813 ± 0.026 μm^{-2} min^{-1}) in a Freiberg Instruments lexsyg research reader. Since it is known that the α-efficiency varies for different chert samples and luminescence emissions (Mercier et al., 1995; Richter and Krbetschek, 2006), it was determined individually for BTL, RTL and OSL.

4.3. Equivalent dose determination

4.3.1. Multiple-aliquot additive-dose (MAAD) measurements (TL)

For MAAD measurements, four dose groups of 4–5 aliquots each received additive β-doses in the range 150–650 Gy prior to TL measurement. After deleting the natural TL by annealing the sample material at 350 °C for 90 min (to reduce potential sensitivity changes) regenerative measurements allowed correcting for the supralinear dose response often observed in the low-dose range (Mercier et al., 1995). To account for inter-aliquot scatter in luminescence sensitivity, we applied the equal pre-dose second-glow normalisation method, that is, every aliquot received the same cumulative dose before the test dose was given (Galloway and Hong, 1996). The sum of equivalent dose (D_e) and supralinearity correction gave the archaeological dose or palaeodose (P) the samples have accumulated during burial. Both quantities resulted from extrapolation of the fitted additive and regenerative dose response curves to the dose axis (Fig. 5). Heating and D_e plateaus indicated the temperature range of thermally stable signals used for dose evaluation and assured that samples were sufficiently heated in the past for TL dating (Aitken, 1985). Examples of TL and dose response curves as well as the D_e plateau of sample SodTL2 are shown in Fig. 5.

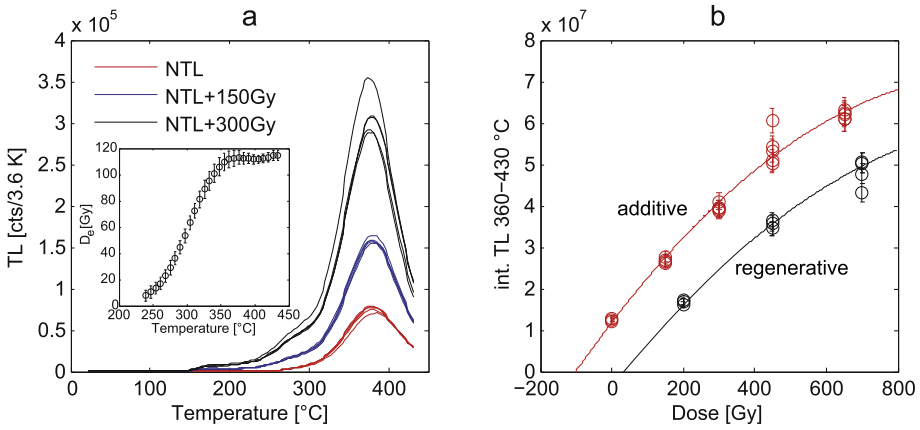

Fig. 5. BTL MAAD measurement results for sample SodTL2. (a) Glow curves of natural aliquots and those having received an additive dose, after second-glow normalisation (not all additive glow curves are shown). The records show the typical TL peak at ~380 °C also observed for samples SodTL0 and SodTL1. The inset shows the calculated D_e as a function of glow temperature (D_e plateau; supralinearity correction not yet included). (b) Additive and regenerative dose response curves, fitted with quadratic functions, using the TL signal of the plateau region (350–410 °C).

4.3.2. Single-aliquot regenerative-dose measurements

4.3.2.1. Thermoluminescence. After sample preparation, a lack of material from sample SodTL0 (<0.5 g) impeded the application of the MAAD protocol routinely used for flint dating (e.g., Mercier et al., 1995). As an alternative, the TL SAR technique theoretically allows determining the palaeodose on one single aliquot and hence requires considerably less sample material. In practice, repeated measurements on several aliquots of a sample are carried out to assess the degree of sample-inherent scatter. Although tested successfully for the RTL emission of flint (Richter and Krbetschek, 2006), the application of the TL SAR procedure generally bears problems such as potentially inappropriate correction for sensitivity changes occurring during repeated irradiation and heating to high temperatures (450 °C in this case). To assess the robustness of this protocol for the present samples, we therefore (1) conducted a dose recovery test (DRT) for each sample and both emissions (BTL, RTL) and (2) compared MAAD ages with TL SAR ages obtained for the same sample (SodTL1 and SodTL2). In addition, we generated both BTL and RTL SAR ages for all three samples, bearing in mind that RTL results are expected to be more accurate due to generally favourable reproducibility of RTL curves during repeated measurements (Fattahi and Stokes, 2000; Richter and Krbetschek, 2006). Sample material for SAR DRT's (both TL and OSL) was annealed at 350 °C for 90 min prior to artificial β-irradiation with a dose in the range of the expected archaeological dose. Each aliquot then received increasing regenerative β-doses with fixed test dose (30 Gy) TL readouts in between (Murray and Wintle, 2000; see also Table 1). The congruence of a repeated dose point with the smallest regenerative dose point ('recycling ratio') served to check for adequate correction of sensitivity changes in the course of the SAR protocol. The sensitivity-corrected dose points (L_x/T_x) were fitted with a single saturating exponential function and the recovered dose was determined through interpolation. SAR measurements of the archaeological dose followed the same protocol, but without annealing and recovery dose. For constructing the dose response curve, the same temperature interval of the glow curve was used as for MAAD analysis. An exemplary dose response curve of sample SodTL0 is shown in Fig. 6.

4.3.2.2. Optically stimulated luminescence. Some chert samples not only yield TL, but also OSL when stimulated with blue light.

Table 1
Protocols used for TL and OSL SAR measurements.

TL SAR[a]	OSL SAR
1. TL to 450 °C → L_n	1. Preheat 260 °C for 10 s
2. Give test dose 30 Gy	2. Stimulate for 80 s at 130 °C → L_n
3. TL to 450 °C → T_n	3. Give test dose 30 Gy
4. Give regeneration dose	4. Cutheat to 240 °C
5. TL to 450 °C → L_x	5. Stimulate for 80 s at 130 °C → T_n
6. Give test dose 30 Gy	6. Stimulate for 80 s at 280 °C ('hot bleach')
7. TL to 450 °C → T_x	7. Give regeneration dose
8. Return to step 4	8. Preheat 260 °C for 10 s
	9. Stimulate for 80 s at 130 °C → L_x
	10. Give test dose 30 Gy
	11. Cutheat to 240 °C
	12. Stimulate for 80 s at 130 °C → T_x
	13. Stimulate for 80 s at 280 °C ('hot bleach')
	14. Return to step 7

[a] The SAR protocol (both for the blue and red emission) includes a background measurement (TL to 450 °C) subsequent to each TL measurement.

Although the general suitability of the flint (chert) OSL signal for dating has been questioned for a long time (e.g., Richter and Temming, 2006), a recent study attests at least part of the investigated chert specimens an OSL emission appropriate for dating (Schmidt and Kreutzer, 2013). Intensive tests on sample SodTL2 proved the long-term stability of its 'fast' OSL component, providing a further, statistically independent dose estimate for this sample ('multi-emission' dating, for detailed discussion and procedures, see Schmidt and Kreutzer, 2013). Samples SodTL0 and SodTL1 do not contain this stable OSL component and are hence not suited for OSL analyses.

To account for recuperation effects, a 'hot bleach' (OSL stimulation at 280 °C for 80 s) was performed after each regeneration cycle (Murray and Wintle, 2003; see also Table 1). Dose response curves were constructed with the OSL signal from the first 0.5 s while subtracting a background derived from the last 20 s of the OSL decay curve. A typical OSL decay curve, dose response curve and $D_e(t)$-plot of sample SodTL2 is shown in Fig. 7. Common rejection criteria (recuperation >5%, recycling ratio outside the range 0.9–1.1; Murray and Wintle, 2000) were applied to select only those aliquots giving valid dose estimates. An OSL DRT with a recovery dose in the range of the expected archaeological dose yielded the best results (dose recovery within <5% deviation) for a preheat temperature of 260 °C (10 s) and a cutheat temperature of

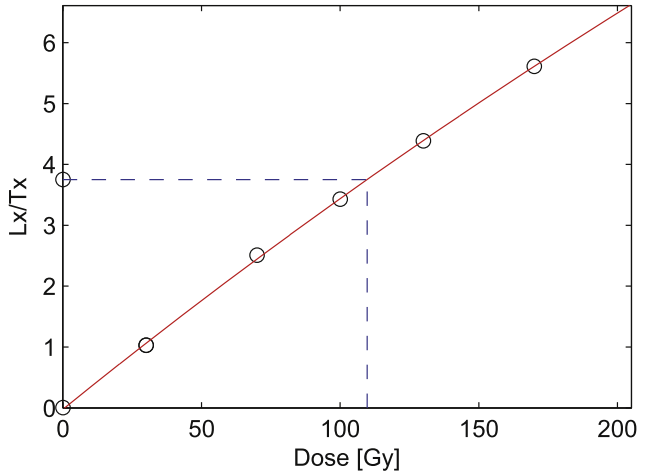

Fig. 6. Typical BTL SAR dose response curve of sample SodTL0. The dose points were fitted with a single saturating exponential function (characteristic saturation dose D_0 = 792 Gy); the resulting archaeological dose is indicated by the dashed blue line and the recycling ratio is 0.99. (For interpretation of the references to colour in this figure legend, the reader is referred to the web version of this article.)

240 °C (see Fig. 6 in Schmidt and Kreutzer, 2013). Samples SodTL0 and SodTL1 only showed an 'ultra-fast'-like OSL component with insufficient thermal stability, so that we did not determine OSL ages for these samples.

4.4. Dose rate assessment

Due to the removal of the outer rim of >2 mm of each chert sample, only cosmic and γ-radiation is relevant for the external dose rate. The γ-contribution of the environmental dose rate was measured *in-situ* in the profile with a γ-probe to account for spatial inhomogeneities in the deposits, mainly caused by limestone boulders fallen from the roof. Additionally, surrounding sediment material was collected for laboratory analysis with high-resolution γ-spectrometry to check for secular disequilibrium in the ^{238}U decay chain. Attenuation of external γ-radiation considering sample shape and mass was carried out with the correction approach of Valladas (1985). For the smallest sample SodTL0, this effect was assumed to be negligible. Rough estimates for SodTL1 – the specimen with the highest internal dose rate – showed that the amount of γ self-dosing is less than ~0.03 Gy ka^{-1} and ignoring it would imply an error in age of <1.5% (Aitken, 1985). The influence of γ self-dosing is henceforth disregarded. The cosmic dose rate was calculated with the formalism implemented in the R-package 'Luminescence' (Kreutzer et al., 2012), following mainly Prescott and Hutton (1994). Considering the shielding from overlying sediments and the roof top, it amounts to 1–2% of the total dose rate at most (Table 2).

Representative, finely ground material of the cores of the chert samples served to determine the internal concentration of K, Th and U by ICP-MS, from which the internal dose rate was calculated according to the conversion factors given in Guérin et al. (2011) and the respective α-efficiency of each sample.

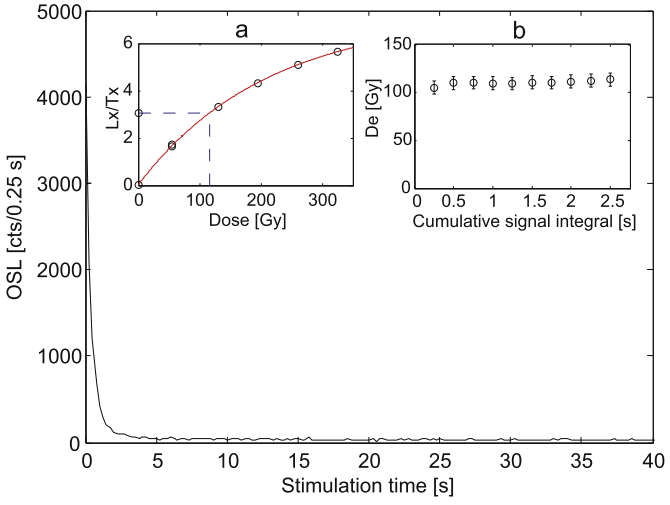

Fig. 7. Typical OSL decay curve of sample SodTL2 (only the first 40 s of a total of 80 s stimulation time are shown for clarity). Inset (a) shows a dose response curve of this sample constructed with the first 0.5 s of the decay curve while subtracting a background of the last 20 s. The dose response curve was fitted with a single saturating exponential function (characteristic saturation dose D_0 = 211 Gy); the resulting archaeological dose is indicated by the dashed blue line and the recycling ratio is 0.96. Inset (b) shows the calculated archaeological dose (D_e) as a function of the cumulative OSL signal integral used for dose response curve construction ($D_e(t)$-plot). The background was always calculated from the last 20 s of the decay curve. (For interpretation of the references to colour in this figure legend, the reader is referred to the web version of this article.)

4.5. Dating results and assessment of consistency

Results of the BTL and RTL SAR DRT are shown in Fig 8. Although within a generally accepted limit of 10% deviation from the given dose, the recovered doses for SodTL0 clearly indicate a trend for dose overestimation using the BTL and RTL SAR protocol. This effect increases for SodTL1 and SodTL2 while data scatter and discrepancy between the blue and red emission also rise. Accordingly, recycling ratio values lying systematically <1 (except BTL of SodTL2) suggest inappropriate correction of sensitivity changes (flattening of dose response curves). While sensitivity changes remained <15% after eight cycles for SodTL0 and SodTL1, they reached up to 30% (RTL) and 45% (BTL) for SodTL2, as evident from test dose monitoring. It is thus questionable whether the TL SAR results of archaeological dose measurements are valid. Moreover, the most severe sensitivity changes often occur in the first heating cycle(s), that is, during archaeological (natural) TL readout. Test dose records may therefore not be a proxy for the sample's sensitivity during the preceding measurement, as is the main condition for application of the SAR protocol. Based on the DRT, a slight overestimation of archaeological dose is expected for BTL and RTL SAR results of SodTL0 and SodTL1 (average dose overestimation of ~8%), if we assume that the amount of sensitivity change is the same for the measurement of the archaeological (natural) signal.

Because of non-correctable sensitivity changes in the course of TL SAR sequences, we consider archaeological doses determined with the MAAD approach as more reliable for the studied samples. The applied normalisation technique effectively reduced the scatter between aliquots of a dose group, and we found no indication of any potential inaccuracies in the context of MAAD palaeodose determination.

Gamma-spectrometry of surrounding sediment indicated the absence of secular disequilibria in the ^{238}U decay chain between ^{226}Ra and ^{214}Bi. Although the organic-rich sediments at Sodmein Cave may be prone to U mobilisation in connection with percolating water, arid climatic conditions during most of the burial time as well as the protected position beneath a rock shelter preclude severe U enrichment or leaching of the cave deposits. The calculated external dose rate deduced from laboratory γ-spectrometry for the three samples is systematically higher than the *in-situ* measured values by about 30–50%. The probable reason for this

Table 2
Analytical data, measurement results and ages of SodTL samples. Only the bold ages are seen as accurate and taken as a basis for discussion of the results, while ages of SodTL0 are clearly maximum ages for reasons discussed in Section 4.5. For further details on the used protocols and calculated ages, see Table 1 and the main text.

Sample	Protocol	Emission	Temperature [°C]	n[a]	Internal radioelement concentration			b-value [Gy μm^2]	$D_{\alpha,\,\mathrm{eff.}}$ [Gy ka^{-1}]	D_β [Gy ka^{-1}]	D_{ext} [Gy ka^{-1}][b]	$D_{\mathrm{ext,\,eff.}}$ [Gy ka^{-1}][c]	D_{total} [Gy ka^{-1}]	D_{intern} [% D_{total}]	Palaeodose [Gy]	Age [ka][g]
					U [ppm]	Th [ppm]	K [wt.%]									
SodTL0	SAR	Blue	380–410	5/5	0.54 ± 0.07	0.23 ± 0.02	0.15 ± 0.005	1.92 ± 0.14	0.248 ± 0.036	0.205 ± 0.011	0.521 ± 0.050	0.499 ± 0.050	0.952 ± 0.067	48	112.8 ± 6.6	**118.5 ± 11.0**
SodTL0	SAR	Red	360–380	11/20	0.54 ± 0.07	0.23 ± 0.02	0.15 ± 0.005	1.24 ± 0.48	0.160 ± 0.068	0.205 ± 0.011	0.521 ± 0.050	0.499 ± 0.050	0.864 ± 0.088	42	104.7 ± 6.4	**121.2 ± 14.8**
SodTL1	MAAD	Blue	360–420	–	2.33 ± 0.30	0.14 ± 0.01	0.08 ± 0.002	1.67 ± 0.17	0.850 ± 0.146	0.407 ± 0.044	0.591 ± 0.050[f]	0.522 ± 0.051	1.779 ± 0.189	71	155.6 ± 8.9[d]	**87.5 ± 9.6**
SodTL1	SAR	Blue	380–410	10/10	2.33 ± 0.30	0.14 ± 0.01	0.08 ± 0.002	1.67 ± 0.17	0.850 ± 0.146	0.407 ± 0.044	0.591 ± 0.050[f]	0.522 ± 0.051	1.779 ± 0.189	71	170.6 ± 9.4	95.9 ± 10.7
SodTL1	SAR	Red	350–390	14/15	2.33 ± 0.30	0.14 ± 0.01	0.08 ± 0.002	1.48 ± 0.45	0.753 ± 0.264	0.407 ± 0.044	0.591 ± 0.050[f]	0.522 ± 0.051	1.682 ± 0.288	69	165.2 ± 9.6	98.2 ± 16.5
SodTL2	MAAD	Blue	360–430	–	1.45 ± 0.19	0.12 ± 0.01	0.14 ± 0.004	1.85 ± 0.25	0.589 ± 0.113	0.326 ± 0.028	0.661 ± 0.050	0.584 ± 0.052	1.500 ± 0.143	61	130.3 ± 8.3[e]	**86.9 ± 9.4**
SodTL2	SAR	Blue	380–410	10/10	1.45 ± 0.19	0.12 ± 0.01	0.14 ± 0.004	1.85 ± 0.25	0.589 ± 0.113	0.326 ± 0.028	0.661 ± 0.050	0.584 ± 0.052	1.500 ± 0.143	61	167.4 ± 9.2	111.6 ± 11.7
SodTL2	SAR	Red	340–380	10/10	1.45 ± 0.19	0.12 ± 0.01	0.14 ± 0.004	1.49 ± 0.17	0.475 ± 0.086	0.326 ± 0.028	0.661 ± 0.050	0.584 ± 0.052	1.385 ± 0.120	58	151.6 ± 11.6	109.5 ± 12.0
SodTL2	SAR (OSL)	UV	–	9/10	1.45 ± 0.19	0.12 ± 0.01	0.14 ± 0.004	0.83 ± 0.13	0.264 ± 0.057	0.326 ± 0.028	0.661 ± 0.050	0.584 ± 0.052	1.175 ± 0.093	50	103.9 ± 7.1	**88.5 ± 8.8**

[a] Number of accepted in relation to measured aliquots.
[b] As measured *in-situ* with the γ-probe and considering a cosmic dose rate of 0.021 ± 0.002 Gy ka^{-1}.
[c] Corrected for influence of moisture content of the sediment and for γ-attenuation within the sample.
[d] Palaeodose value includes a supralinearity correction of 20.8 ± 5.2 Gy.
[e] Palaeodose value includes a supralinearity correction of 17.4 ± 4.4 Gy.
[f] Value based on interpolation and Mercier et al. (1999).
[g] Given with uncertainty at 1-σ confidence level.

deviation can be seen in the limestone boulders and rocks (poor in radionuclides) that are present in the profile, but not in the sample material analysed by γ-spectrometry. Since the measurements conducted directly at the find spots are seen as representing more closely the radiation actually received by the samples and since these values are in agreement with the data collected by Mercier et al. (1999) (*in-situ* with $CaSO_4$:Dy dosimeters), age calculations are based on *in-situ*-measured dose rates.

Analytical results, calculated dose rates, palaeodoses and resulting ages are summarised in Table 2. Based on experience from the DRT, the BTL and RTL SAR ages of 119 ± 11 ka and 121 ± 15 ka of sample SodTL0 most likely represent maximum ages (due to dose overestimation of the applied protocol). These ages agree within uncertainty with those obtained previously (averaged at 118 ± 8 ka; Mercier et al., 1999), but SodTL0 originates from a layer stratigraphically below the 1993/1995 samples. For SodTL1, SAR ages of 96 ± 11 ka (BTL) and 98 ± 17 ka (RTL) are higher than the MAAD age (88 ± 10 ka), but still coincide at 1-σ level. In contrast, significantly older SAR ages result from BTL (112 ± 12 ka) and RTL (110 ± 12 ka) SAR for SodTL2 in comparison to MAAD (87 ± 9 ka) and OSL SAR (89 ± 9 ka) ages. All data considered as trustworthy on the basis of the conducted accuracy checks are concordant (i.e., MAAD and OSL SAR), stratigraphically consistent and fall between 87 and 89 ka (see bold ages in Table 2). It is interesting to note that the deviation between recovered and given dose in the DRT (i.e., the accuracy of dose recovery) appears to correlate with the difference in MAAD and SAR TL ages. For instance, sample SodTL2 shows both the worst dose recovery ratio and the largest variance between MAAD and SAR ages, while both figures are smaller for SodTL1.

The 'multi-emission' dating approach (several ages for the same sample) applied here served as a further check for the accuracy and internal validity of the obtained dates (Westaway and Prescott, 2012). These individual ages may be considered as self-contained since different types of electron traps and recombination centres (e.g., blue MAAD vs. UV OSL) participate in the luminescence process. If consistent, multiple ages may thus provide reassurance of dating results and may help identify unstable emissions or other systematic errors in case of age discrepancies. This approach, however, does apply only for the issue of palaeodose determination, as the multiple ages generated for each sample share the same dose rate (except for the α-contribution) and hence (potentially) the same associated errors.

5. Discussion and conclusions

We showed here that the parallel application of different measurement protocols and the use of several luminescence emissions of chert allow the critical re-assessment of obtained dates and contributes to identifying ages clearly affected by systematic errors. In this case, TL SAR ages proved to be overestimated and archaeological interpretation should therefore be based on TL MAAD and OSL SAR ages instead. However, the precise chronological interpretation of the fire pit sequence turns out to be difficult. We consider that the earliest hearth phase is constrained by the maximum ages of SodTL0. They are remarkably similar to the 118 ± 8 ka average obtained by Mercier et al. (1999), but our present analysis strongly suggests that those samples are associated with the overlying middle hearth. In its turn, sample SodTL1 which is associated with the same event provides a more recent TL MAAD age. Is this an incentive to re-question the stratigraphic association of the original samples? At least in the case of ME95/56 this is not possible: its association with the middle hearth is beyond doubt. The MAAD ages of SodTL1 and SodTL2 are identical. Given that the two burning phases of the

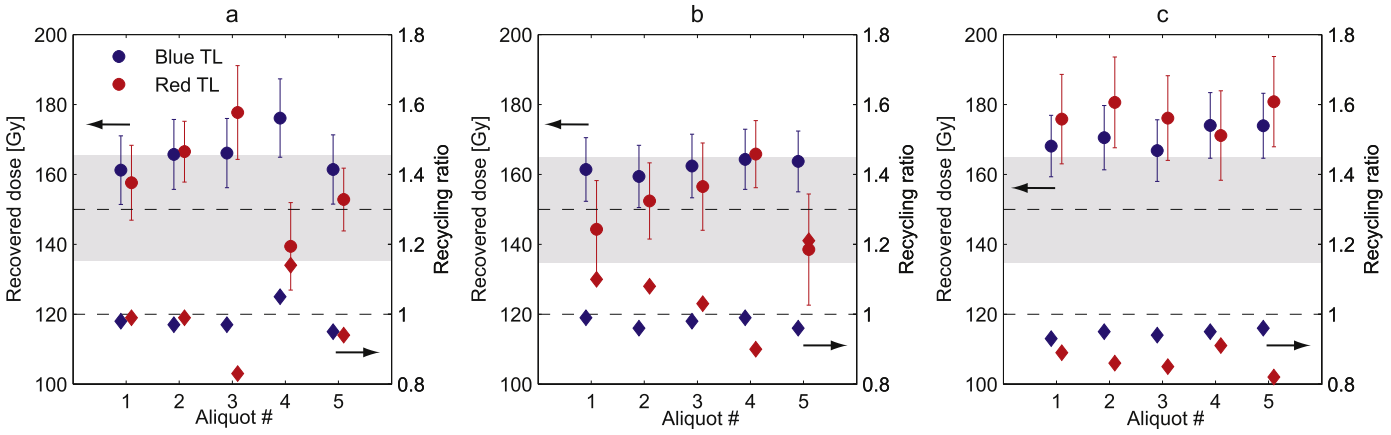

Fig. 8. Results of the BTL and RTL SAR dose recovery test for SodTL0 (a), SodTL1 (b) and SodTL2 (c). Five aliquots were measured per sample and recorded emission. The left ordinate indicates the recovered dose (circles), while the right ordinate shows the recycling ratio (diamonds). The dashed lines represent the given dose (150 Gy) and a recycling ratio of 1, respectively. The shaded area represents the ±10% error margins of dose recovery.

middle hearth are stratigraphically separated by an erosional event, the interpretation that SodTL2 derives from the older phase seems more likely than the alternative of a relatively short duration for the middle hearth.

Hence, the newly measured luminescence ages of these stratigraphically secure samples appear to indicate that the fire pit has been used and re-used during a significant period of time. This is in good agreement with the stratigraphic evidence of its initial use during the sedimentation of layer J and its final re-cutting from a topographic surface contained in layer I.

In summary, Sodmein Cave yields an exceptional archaeological stratigraphy of human occupation debris ranging from at least MIS 5 until the Holocene and, hence, its investigation promises further insights for the 'Out of Africa II' debate. On this account, future interdisciplinary efforts of the project will comprise excavations and geo-archaeological surveys in Sodmein Cave in order to investigate the complete archaeological inventory and the sedimentological sequence of the cave. Beside detailed archaeological and geomorphological research, it is planned to take further samples for dating.

Acknowledgements

"Sodmein Cave", the excavation concession of which is held by the University of Leuven (Belgium), is a joint research project of the Universities of Cologne (Germany) and Leuven, under the aegis of the Collaborative Research Centre (CRC 806) "Our Way to Europe". This research centre, focusing on the culture-environment interaction and the human mobility in the Late Quaternary, is generously funded by the Deutsche Forschungsgemeinschaft (DFG). For the fieldwork the joint geo-archaeological team established a close collaboration with the geologists of the Egyptian Mineral Resources Authority (EMRA) and the archaeologists of the Ministry of State for Antiquities (MSA). We are obliged to both organisations for the permission to carry out geo-archaeological work in the cave and for the practical support in the field.

References

Aitken, M.J., 1985. Thermoluminescence Dating. Academic Press, London.
Beyin, A., 2011. Upper Pleistocene human dispersals out of Africa: a review of the current state of the debate. Int. J. Evol. Biol. 2011, 1–17.
Bowman, S., Huntley, D., 1984. A new proposal for the expression of alpha efficiency in TL dating. Anc. TL 2, 6–8.
Derricourt, R., 2006. Getting "Out of Africa": sea crossings, land crossings and culture in the Hominin Migrations. J. World Prehistory 19, 119–132.
Fattahi, M., Stokes, S., 2000. Extending the time range of luminescence dating using red TL (RTL) from volcanic quartz. Radiat. Meas. 32, 479–485.
Galloway, R., Hong, D., 1996. Concerning the normalization of additive dose optically stimulated luminescence data from quartz. Anc. TL 14, 1–5.
Grove, M., 2015. Palaeoclimates, plasticity, and the early dispersal of *Homo sapiens*. Quat. Int. 369, 17–37.
Guérin, G., Mercier, N., Adamiec, G., 2011. Dose-rate conversion factors: update. Anc. TL 29, 5–8.
Kindermann, K., Bubenzer, O., Van Peer, P., September 2013. Geo-archaeological research on the Late Pleistocene of the Egyptian Eastern Desert: recent threats to the Sodmein Cave. Antiq. Proj. Gallery 337.
Kreutzer, S., Schmidt, C., Fuchs, M.C., Dietze, M., Fischer, M., Fuchs, M., 2012. Introducing an R package for luminescence dating analysis. Anc. TL 30, 1–8.
Mercier, N., Valladas, H., Valladas, G., 1995. Flint thermoluminescence dates from the CFR laboratory at Gif: contributions to the study of the chronology of the Middle Palaeolithic. Quat. Sci. Rev. 14, 351–364.
Mercier, N., Valladas, H., Froget, L., Joron, J.-L., Vermeersch, P., Van Peer, P., Moeyersons, J., 1999. Thermoluminescence dating of a middle palaeolithic occupation at sodmein cave, Red Sea Mountains (Egypt). J. Archaeol. Sci. 26, 1339–1345.
Moeyersons, J., Vermeersch, P.M., Van Peer, P., 2002. Dry cave deposits and their palaeoenvironmental significance during the last 115 ka, Sodmein Cave, Red Sea Mountains, Egypt. Quat. Sci. Rev. 21, 837–851.
Murray, A.S., Wintle, A.G., 2000. Luminescence dating of quartz using an improved single-aliquot regenerative-dose protocol. Radiat. Meas. 32, 57–73.
Murray, A.S., Wintle, A.G., 2003. The single aliquot regenerative dose protocol: potential for improvements in reliability. Radiat. Meas. 37, 377–381.
Pagani, L., Schiffels, S., Gurdasani, D., Danecek, P., Scally, A., Chen, Y., Xue, Y., Haber, M., Ekong, R., Oljira, T., Mekonnen, E., Luiselli, D., Bradman, N., Bekele, E., Zalloua, P., Durbin, R., Kivisild, T., Tyler-Smith, C., 2015. Tracing the route of modern humans out of Africa by using 225 human genome sequences from Ethiopians and Egyptians. Am. J. Hum. Genet. 96, 986–991.
Prescott, J.R., Hutton, J.T., 1994. Cosmic ray contributions to dose rates for luminescence and ESR dating: large depths and long-term time variations. Radiat. Meas. 23, 497–500.
Prickett, M., Whitcomb, D., Johnson, J. (Eds.), 1979. Quseir Regional Survey. Quseir Al-qadim 1978 Preliminary Report. American Research Centre in Egypt, pp. 257–349.
Richter, D., Krbetschek, M., 2006. A new thermoluminescence dating technique for heated flint. Archaeometry 48, 695–705.
Richter, D., Temming, H., 2006. Testing heated flint palaeodose protocols using dose recovery procedures. Radiat. Meas. 41, 819–825.
Richter, D., Tostevin, G., Škrdla, P., Davies, W., 2009. New radiometric ages for the Early Upper Palaeolithic type locality of Brno-Bohunice (Czech Republic): comparison of OSL, IRSL, TL and ^{14}C dating results. J. Archaeol. Sci. 36, 708–720.
Schmidt, C., 2013. Luminescence Dating of Heated Silex – Potential to Improve Accuracy and Precision and Application to Paleolithic Sites (PhD thesis). University of Cologne.
Schmidt, C., Kreutzer, S., 2013. Optically stimulated luminescence of amorphous/microcrystalline SiO_2 (silex): basic investigations and potential in archeological dosimetry. Quat. Geochronol. 15, 1–10.
Valladas, H., 1985. Datation par la thermoluminescence de gisements moustériens du sud de la France (PhD thesis). Université Paris VI.
Valladas, H., 1992. Thermoluminescence dating of flint. Quat. Sci. Rev. 11, 1–5.

Van Peer, P., 1998. The nile corridor and the out-of Africa model. An examination of the archaeological record. Curr. Anthropol. 39 (Suppl.), 115–140.
Van Peer, P., Vermeersch, P.M., 2000. The Nubian complex and the dispersal of modern humans in North Africa. In: Krzyzaniak, L., Kröper, K., Kobusiewicz, M. (Eds.), Recent Research into the Stone Age of Northeastern Africa. Studies in African Archaeology 7, Poznan, pp. 47–60.
Vermeersch, P.M. (Ed.), 2002. Palaeolithic Quarrying Sites in Upper and Middle Egypt. Egyptlan Prehistory Monographs 4. Leuven University Press, Leuven.
Vermeersch, P.M., Van Peer, P., Moeyersons, J., Van Neer, W., 1994. Sodmein cave site, Red Sea Mountains (Egypt). Sahara 6, 31–40.
Westaway, K., Prescott, J., 2012. Investigating signal evolution: a comparison of red and UV/blue TL, and UV OSL emissions from the same quartz sample. Radiat. Meas. 47, 909–915.
Wurz, S., Van Peer, P., 2012. Out of Africa, the Nile Valley and the Northern route. South Afr. Archaeol. Bull. 67, 168–179.